

# UCSF

## UC San Francisco Previously Published Works

### Title

Multimodality Imaging of Ethiodized Oil-loaded Radiopaque Microspheres during Transarterial Embolization of Rabbits with VX2 Liver Tumors.

### Permalink

<https://escholarship.org/uc/item/8ts622n1>

### Journal

Radiology, 279(3)

### ISSN

0033-8419

### Authors

Tacher, Vania  
Duran, Rafael  
Lin, MingDe  
[et al.](#)

### Publication Date

2016-06-01

### DOI

10.1148/radiol.2015141624

Peer reviewed

# Multimodality Imaging of Ethiodized Oil–loaded Radiopaque Microspheres during Transarterial Embolization of Rabbits with VX2 Liver Tumors<sup>1</sup>

Vania Tacher, MD  
 Rafael Duran, MD  
 MingDe Lin, PhD  
 Jae Ho Sohn, MS, MD  
 Karun V. Sharma, MD  
 Zhijun Wang, MD, PhD  
 Julius Chapiro, MD, PhD  
 Carmen Gacchina Johnson, PhD  
 Nikhil Bhagat, MD  
 Matthew R. Dreher, PhD  
 Dirk Schäfer, PhD  
 David L. Woods, MS  
 Andrew L. Lewis, PhD  
 Yiqing Tang, PhD  
 Michael Grass, PhD  
 Bradford J. Wood, MD  
 Jean-François Geschwind, MD

<sup>1</sup>From the Russell H. Morgan Department of Radiology and Radiological Science, Division of Vascular and Interventional Radiology, Johns Hopkins Hospital, Baltimore, Md (V.T., R.D., J.H.S., Z.W., J.C., N.B., J.F.G.); Department of Radiology, Yale University School of Medicine, 330 Cedar St, TE 2-230, New Haven, CT 06520 (R.D., J.H.S., J.C., J.F.G.); U/S Imaging and Interventions (UII), Philips Research North America, Cambridge, Mass (M.L.); Center for Interventional Oncology, Interventional Radiology Section, National Institutes of Health, Bethesda, Md (K.V.S., C.G.J., M.R.D., D.L.W., B.J.W.); Biocompatibles UK Ltd, Farnham, Surrey, England (M.R.D., A.L.L., Y.T.); and Philips Research Hamburg, Hamburg, Germany (D.S., M.G.). Received July 23, 2014; revision requested September 12; revision received June 17, 2015; accepted July 31; final version accepted September 21. **Address correspondence to** J.F.G. (e-mail: [jeff.geschwind@yale.edu](mailto:jeff.geschwind@yale.edu)).

Supported by the French Society of Radiology, Philips Research North America, and Biocompatibles UK Ltd. This research was supported by the National Institutes of Health (grant R01 CA160771).

V.T. and R.D. contributed equally to this work.

© RSNA, 2015

## Purpose:

To assess the visibility of radiopaque microspheres during transarterial embolization (TAE) in the VX2 rabbit liver tumor model by using multimodality imaging, including single-snapshot radiography, cone-beam computed tomography (CT), multidetector CT, and micro-CT.

## Materials and Methods:

The study was approved by the institutional animal care and use committee. Fifteen VX2-tumor-bearing rabbits were assigned to three groups depending on the type of embolic agent injected: 70–150- $\mu$ m radiopaque microspheres in saline (radiopaque microsphere group), 70–150- $\mu$ m radiopaque microspheres in contrast material (radiopaque microsphere plus contrast material group), and 70–150- $\mu$ m radiolucent microspheres in contrast material (nonradiopaque microsphere plus contrast material group). Rabbits were imaged with single-snapshot radiography, cone-beam CT, and multidetector CT. Three to 5 weeks after sacrifice, excised livers were imaged with micro-CT and histologic analysis was performed. The visibility of the embolic agent was assessed with all modalities before and after embolization by using a qualitative three-point scale score reading study and a quantitative assessment of the signal-to-noise ratio (SNR) change in various regions of interest, including the tumor and its feeding arteries. The Kruskal-Wallis test was used to compare the rabbit characteristics across groups, and the Wilcoxon signed rank test was used to compare SNR measurements before and after embolization.

## Results:

Radiopaque microspheres were qualitatively visualized within tumor feeding arteries and targeted tissue with all imaging modalities ( $P < .05$ ), and their presence was confirmed with histologic examination. SNRs of radiopaque microsphere deposition increased after TAE on multidetector CT, cone-beam CT, and micro-CT images ( $P < .05$ ). Similar results were obtained when contrast material was added to radiopaque microspheres, except for additional image attenuation due to tumor enhancement. For the group with nonradiopaque microspheres and contrast material, retained tumoral contrast remained qualitatively visible with all modalities except for micro-CT, which demonstrated soluble contrast material washout over time.

## Conclusion:

Radiopaque microspheres were visible with all imaging modalities and helped increase conspicuity of the tumor as well as its feeding arteries after TAE in a rabbit VX2 liver tumor model.

© RSNA, 2015

**H**epatocellular carcinoma is the fifth most common cancer worldwide and the second most common cause of cancer-related death (1,2). Because of the often advanced stage of the disease at diagnosis, less than 25% of patients are candidates for tumor resection or orthotopic liver transplantation (3,4). Thus, local-regional treatments are the mainstay of therapy for many patients with unresectable disease (5–8). The most widely used type of transcatheter arterial chemoembolization (TACE) is conventional TACE. This procedure involves the injection of an emulsion of various chemotherapeutic drugs such as doxorubicin, mitomycin, and/or cisplatin mixed with ethiodized oil. This ethiodized oil (Lipiodol Ultra-Fluide; Guerbet, Villepinte, France [480 mg of iodine per milliliter]) functions as an imaging contrast material owing to its radiopacity and is mainly used as a drug carrier to locally deliver chemotherapeutic agents directly to the tumor (9–12).

Less than a decade ago, a new drug delivery system, drug-eluting beads, was introduced with the goal of improving local drug delivery and limiting or further minimizing systemic exposure of chemotherapeutic agents (13–17). TACE with drug-eluting beads uses calibrated spherical microspheres loaded with chemotherapeutic drugs, which are injected directly into tumor-feeding arteries. This form of treatment brings about the dual benefit of cytotoxic and embolic effects and, compared with conventional TACE, has demonstrated a better tumor response, a delay in tumor progression, and fewer side effects (18–21). However, a substantial drawback of these microspheres is that they are radiolucent, and so they are routinely mixed with soluble radiologic

contrast material for indirect visualization and monitoring under real-time fluoroscopy during delivery. However, it is the column of contrast material rather than the microspheres themselves that is being imaged. Moreover, transient contrast material saturation of the tumor or tumor devascularization is the only intraprocedural indication of treatment success as evidenced with different cone-beam computed tomography (CT) techniques (22,23). This may not represent the exact location of drug elution. Thus, the lack of direct intraprocedural feedback is a limitation of TACE with drug-eluting beads and can potentially contribute to nontarget embolization and complications (24,25). To address the lack of direct radiologic visibility, radiopaque microspheres loaded with ethiodized oil have recently been developed (13,26).

The purpose of our study was to assess the visibility of the radiopaque microspheres during transarterial embolization (TAE) in the VX2 rabbit liver tumor model by using multimodality imaging, including single-snapshot radiography, cone-beam CT, multidetector CT, and micro-CT.

### Materials and Methods

The study was performed with financial support from the National Institutes of

### Implications for Patient Care

- Ethiodized oil–loaded radiopaque microspheres may enable direct image feedback to intraprocedurally guide embolization and potentially mitigate nontarget embolization.
- Visibility of the ethiodized oil–loaded radiopaque microspheres is maintained after the procedure, which enables postprocedure verification of bead deposition; patient care may be optimized accordingly (eg, identification of nontarget embolization), and the location of the radiopaque microsphere may provide information for planning the next treatment cycle.

Health (NIH/NCI R01 CA160771), the French Society of Radiology, Philips Research, and Biocompatibles UK. Authors who were not funded by the sponsors (V.T., R.D., J.H.S., K.V.S., Z.W., J.C., C.G.J., N.B., D.L.W., B.J.W., J.F.G.) had full control of the data and their analysis during the entire study. The experiments were performed while M.R.D. was at the Center for Interventional Oncology at the National Institutes of Health; M.R.D. is now a paid employee of Biocompatibles. M.L., D.S., and M.G. are employees of Philips, and M.R.D., A.L., and Y.T. are employees of Biocompatibles. B.J.W., A.L., and Y.T. are coinventors on a filed patent related to this work (27).



### Study Population

Our study was approved by the institutional animal care and use committee, and all animal care and use procedures were performed under regulatory guidelines. A total of 18 adult New Zealand White male rabbits (Myrtle's Rabbitry, Thompson Station, Tenn) weighing 3.8–4.3 kg were used for our study. Three rabbits were used as tumor carriers and 15 underwent implantation of VX2 tumors into the left

### Advance in Knowledge

- Ethiodized oil–loaded radiopaque microspheres (70–150  $\mu$ m) were visible with multiple radiologic imaging modalities during transarterial embolization in a VX2 tumor liver model, even after soluble iodinated contrast material washout.

### Published online before print

10.1148/radiol.2015141624 Content codes:  

Radiology 2016; 279:741–753

### Abbreviations:

ROI = region of interest  
 SNR = signal-to-noise ratio  
 TACE = transcatheter arterial chemoembolization  
 TAE = transarterial embolization

### Author contributions:

Guarantors of integrity of entire study, V.T., Z.W., C.G.J., N.B., J.F.G.; study concepts/study design or data acquisition or data analysis/interpretation, all authors; manuscript drafting or manuscript revision for important intellectual content, all authors; manuscript final version approval, all authors; agrees to ensure any questions related to the work are appropriately resolved, all authors; literature research, V.T., R.D., M.L., J.H.S., K.V.S., J.C., N.B., M.G., B.J.W., J.F.G.; experimental studies, V.T., R.D., M.L., K.V.S., Z.W., J.C., C.G.J., M.R.D., D.S., D.L.W., A.L.L., Y.T., M.G., B.J.W., J.F.G.; statistical analysis, V.T., M.L., J.H.S., K.V.S., M.R.D., J.F.G.; and manuscript editing, V.T., R.D., M.D.L., J.H.S., K.V.S., J.C., N.B., M.R.D., D.L.W., A.L.L., Y.T., B.J.W., J.F.G.

Conflicts of interest are listed at the end of this article.

liver lobe before embolization. These rabbits were then randomly assigned to one of three groups (five rabbits in each group). The first group underwent TAE with radiopaque microspheres (0.2 mL) suspended in saline (4 mL) (radiopaque microsphere group), the second group underwent TAE with radiopaque microspheres (0.2 mL) diluted in soluble contrast material (2 mL of saline and 2 mL of iohexol [300 mg of iodine per milliliter]) (radiopaque microsphere plus contrast material group), and the third group underwent TAE with nonradiopaque microspheres (0.2 mL of 70–150- $\mu\text{m}$  LC-BeadM1 [Biocompatibles, Farnham, England]) diluted in soluble contrast material (2 mL of saline and 2 mL of iohexol [300 mg of iodine per milliliter]) (nonradiopaque microsphere plus contrast material group). A summary of the group characteristics is given in Table 1.

### Radiopaque Microspheres

Acrylamido-polyvinyl alcohol-co-acrylamido-2-methylpropane sulfonate microspheres were provided for this study in sterile, vacuum-sealed vials by Biocompatibles UK. We used 70–150- $\mu\text{m}$  microspheres because this size is appropriate for the rabbit model. LC-BeadM1 microspheres (70–150  $\mu\text{m}$ ) were lyophilized in the presence of mannitol. Mannitol served as a matrix-forming additive, creating an amorphous phase in the spaces vacated by the water during lyophilization. Upon hydration, the excipient rapidly dissolves as the hydrogel reforms the swollen, compressible embolization microspheres (approximately 2 mL of microspheres per vial). Ethiodized oil was loaded into the lyophilized microspheres as follows: (a) A total of 4 mL of a 15:1 mixture of ethiodized oil to ethanol was added to a vial of 70–150- $\mu\text{m}$  dry microspheres while maintaining vacuum in the vial and allowed to incubate for 30 minutes at room temperature. (b) After ethiodized oil incubation, 10 mL of sterile water was added to the vial, the vial was gently agitated, and the unloaded ethiodized oil was allowed to settle to the bottom of the vial. Unloaded ethiodized oil was then

**Table 1**

#### Summary of Group Characteristics

Group and Rabbit No.	Tumor Size (cm)	Total Volume Injected (mL)	Total Packed Bead Volume Injected (mL)	Catheter Position
<b>Radiopaque microsphere</b>				
1A	3.5	1	0.05	CHA
1B	2	4.5	0.225	PHA
1C	3.4	6	0.3	PHA
1D	3	6	0.3	CHA
1E	2.5	6	0.3	PHA
<b>Radiopaque microsphere plus contrast material</b>				
2A	2.7	1	0.05	LHA
2B	4.4	1	0.05	LHA
2C	1.9	1	0.05	PHA
2D	1.3	2.5	0.125	LHA
2E	4.1	4	0.2	PHA
<b>Nonradiopaque microsphere plus contrast material</b>				
3A	4.9	6	0.3	PHA
3B	1.6	20	1	CHA
3C	3.8	4.5	0.225	PHA
3D	3.5	3	0.15	PHA
3E	2.7	6	0.3	PHA

Note.—CHA = common hepatic artery, LHA = left hepatic artery, PHA = proper hepatic artery. *P* values from comparison of the three groups were as follows: tumor size: .76, total volume injected: .03, total packed beads: .03.

carefully removed by using a needle and syringe. (c) Five additional washing steps were repeated by using 10 mL of sterile water and gently passing the ethiodized oil–loaded microspheres back and forth through a metal three-way stopcock connected to two glass syringes. During each washing step, the microspheres were allowed to settle in one syringe and the excess solution containing ethiodized oil was removed from the second syringe. The ethiodized oil–loaded microspheres were then ready for use for embolization (13,26).

### Tumor Implantation

All surgical procedures were performed by a resident in radiology (V.T.), an interventional radiologist (R.D., with 8 years of experience) who specialized in abdominal imaging with experience with the rabbit model, and an author with PhD with 2 years of experience with rabbits (C.G.J.). Each rabbit was placed in the supine position, prepared, and draped in a sterile

fashion. Anesthesia was induced with 5% isoflurane (Hospira, Warwickshire, England) and 95% oxygen (Air Gas, Salem, NH) and then sustained with 2.5% isoflurane and 97.5% oxygen at a rate of 3.5 L/min, with intravenous bolus injections of 0.25 mL propofol (10 mg/mL) (APP Pharmaceuticals, Schaumburg, Ill) via a marginal ear vein. Chunks of VX2 tumor were excised from the hind legs of the carriers, minced, and surgically implanted into the left lobe of the liver as previously described (28). The liver tumors were monitored with ultrasonography (SonoSite 180 PLUS; SonoSite, Bothell, Wash) and allowed to grow for 12–15 days after tumor implantation to reach dimensions of 2–3 cm.

### TAE and Intraoperative Imaging

All TAE procedures were performed by two of the authors who performed the surgical procedures (V.T. and R.D.) and an interventional radiologist with experience with the rabbit model (K.V.S.,

with 10 years of experience). Each rabbit was anesthetized in the same way as for tumor implantation. Surgical cut-down was performed to gain access to the common femoral artery, into which a 3-F sheath (Cook, Bloomington, Ind) was placed. A specially manufactured 2-F catheter with a tip in the shape of a hockey stick (JB1 catheter, Cook) and a 0.014-inch guide wire (Transcend; Boston Scientific, Natick, Mass) were used to catheterize the celiac axis, after which celiac and common hepatic arteriograms were obtained with contrast material (iohexol, 300 mg of iodine per milliliter) to delineate the blood supply to the liver and to confirm the location of the tumor and its tumor-feeding arteries.

All intraprocedural imaging was performed by using a C-arm system (Allura FD20; Philips Healthcare, Best, the Netherlands) that allows acquisition of fluoroscopy (three frames per second; 85 kVp; 23 mA; duration of x-ray exposure, 45 msec; binning,  $2 \times 2$ ), single-snapshot radiography (70 kVp; 23 mA; duration of x-ray exposure, 45 msec; binning,  $1 \times 1$ ; pixel,  $0.154 \times 0.154$  mm), cone-beam CT

(30 frames per second; 324 images; 80 kVp; 50 mA; duration of x-ray exposure, 3 msec; resolution,  $0.98 \times 0.98 \times 0.98$  mm<sup>3</sup>; field of view,  $25 \times 25 \times 19$  cm; matrix size,  $256 \times 256 \times 198$  mm), and navigation. Digital subtraction angiography was performed during injection of soluble contrast material to identify the tumor blush before embolization. After having ensured adequate positioning of the catheter as close as possible to the tumor while maintaining adequate flow in the selected feeding artery (common, proper, or left hepatic artery), a minimum of 20 minutes was allowed to elapse, during which saline was intermittently flushed through the catheter to ensure adequate washout of the contrast material used during catheterization. Once the washout was confirmed with all intraprocedural imaging modalities, baseline pre-embolization fluoroscopy, single-snapshot radiography, and cone-beam CT were performed.

The tumor was embolized under real-time fluoroscopy with alternating injections of 0.05-mL aliquots of embolic agent (approximately 0.01 mL per 5 seconds) and saline. Intermittent

single-snapshot radiographs were acquired after each saline flush. The end point of the embolization procedure was the advent of left lobar arterial inflow reduction with the identification of reflux of the embolic agent (ie, nontarget embolization). These angiographic findings were thought to reflect saturation of the tumor and its feeding arteries with microspheres. Unenhanced cone-beam CT was performed immediately after completion of the infusion. At the end of the embolization, the catheter was removed and the common femoral artery was ligated by using suture material to obtain hemostasis. One hour after TAE and while still sedated, all rabbits underwent unenhanced multidetector CT (Aquilion One; Toshiba, Tokyo, Japan) with the following parameters: 120 kVp; 80 mA; rotation time, 0.5 second; scanning time, 60.5 seconds; matrix,  $512 \times 512 \times 200$  mm; and reconstructed field of view,  $492 \times 492 \times 192$  mm.

### Ex Vivo Imaging

After postprocedural multidetector CT, the rabbits were immediately euthanized under deep anesthesia with

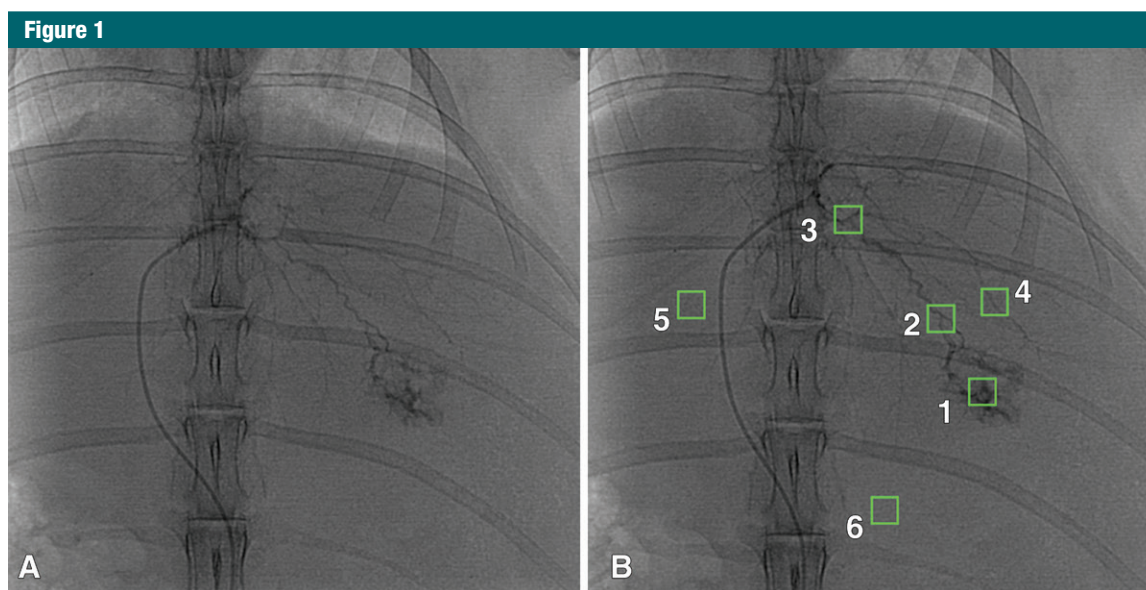


**Figure 1:** A, Single-snapshot image obtained at embolization end point in rabbit treated with radiopaque microspheres diluted in soluble contrast material (radiopaque microsphere plus contrast material group). B, Single-snapshot image shows regions of interest (ROIs) (in green) used for SNR calculation. 1 = tumor, 2 = tumor-feeding arteries, 3 = proximal left hepatic artery, 4 = ipsilateral liver, 5 = contralateral liver. ROI 6 was used to calculate noise.

intravenous injection of 10 mL of propofol (10 mg/mL). The liver was carefully harvested and immediately imaged with cone-beam CT with the following parameters: 80 kVp; 85 mA; duration of x-ray exposure, 5 msec; 30 frames per second; 624 images; matrix, 256 × 256 × 198 mm; and field of view, 25 × 25 × 19 cm. The liver was then placed in a container with a 10% buffered formaldehyde solution. The liver of one rabbit in each group was then imaged again with cone-beam CT by using the same scanning parameters at 3 and 7 days after TAE to investigate bead visibility and contrast material washout over time.

Three to 5 weeks later, the visibility of microspheres in the excised left liver lobes was evaluated by using a high-spatial-resolution micro-CT 100 unit (Scanco Medical, Bruttisellen, Switzerland) with the following parameters: 90 kVp, 400-msec integration time, 88 mA, and 17- $\mu\text{m}^2$  voxel resolution (D.L.W., with 7 years of experience).

**Histologic Analysis**

Approximately 1 week after micro-CT, careful dissection of the explanted liver was performed and the tumor (from the periphery to the opposite border) and nontumor tissues (right lobe) were taken for pathologic examination. The tissues were cut and prepared into five paraffin blocks that were each 500  $\mu\text{m}$  thick. From each block, 5- $\mu\text{m}$ -thick slices were made with a microtome, and each slice was stained with hematoxylin and eosin. The sections were scanned and imaged with an Aperio Image Scope system (Aperio Technologies, Vista, Calif) to perform histologic analysis. Histologic analysis enabled the determination of the microsphere location (tumor, tumor rim, feeding arteries, and peritumoral hepatic parenchyma) and was considered the standard of reference for our study. A three-point scale was used to qualitatively assess the amount of microspheres, as follows: 1 = no microspheres, 2 = fewer than three microspheres per site and per slice examined, and 3 = more than three microspheres per slice examined.

**Data Analysis**

Data analysis involved qualitative and quantitative image analysis and pathologic examination. Image analysis was performed by using free viewer software (OsiriX 5.7; OsiriX Foundation,

Geneva, Switzerland). The maximum tumor diameter was measured on axial pre-TAE unenhanced cone-beam CT images (by a radiology resident [V.T.]). Evaluation of embolic agent visibility was performed by using projection

**Table 2**

**Qualitative and Quantitative Visibility according to Anatomic Location**

Anatomic Location and Group	No. of Definitely Visible Cases at Image Assessment			SNR Measurements		
	Before Embolization*	After Embolization*†	P Value	Median SNR Change (%)	No. of Cases with SNR Improvement*	P Value‡
<b>Tumor</b>						
Radiopaque microsphere	0/60	41/60 (68)	<.001	7.3	15/20	.036
Radiopaque microsphere plus contrast material	0/60	46/60 (77)	<.001	41.1	18/20	.004
Nonradiopaque microsphere plus contrast material	0/60	26/60 (43)	<.001	21.6	13/20	.287
<b>Feeding artery</b>						
Radiopaque microsphere	0/60	34/60 (57)	<.001	21.8	14/20	.024
Radiopaque microsphere plus contrast material	0/60	43/60 (72)	<.001	25.3	13/20	.006
Nonradiopaque microsphere plus contrast material	0/60	18/60 (30)	<.001	10.3	15/20	.614
<b>Surrounding liver</b>						
Radiopaque microsphere	0/60	36/60 (60)	<.001	-0.3	15/20	.824
Radiopaque microsphere plus contrast material	0/60	34/60 (57)	<.001	2.7	12/20	.365
Nonradiopaque microsphere plus contrast material	0/60	21/60 (35)	<.001	0.3	16/20	.695
<b>Hepatic arteries</b>						
Radiopaque microsphere	0/60	45/60 (75)	<.001	32.4	9/20	.002
Radiopaque microsphere plus contrast material	0/60	37/60 (62)	<.001	20.7	10/20	.006
Nonradiopaque microsphere plus contrast material	0/60	22/60 (37)	<.001	2.5	12/20	.888
<b>Nontarget embolization in contralateral lobe<sup>§</sup></b>						
Radiopaque microsphere	0/45	31/45 (69)	<.001	42.6	9/15	.004
Radiopaque microsphere plus contrast material	0/45	25/45 (56)	<.001	23.5	8/15	.048
Nonradiopaque microsphere plus contrast material	0/45	27/45 (60)	<.001	4.7	9/15	.477

\* Numbers are raw data.

† Numbers in parentheses are percentages.

‡ Comparison of SNR measurements before and after TAE.

§ Evaluation of nontarget embolization was not performed with micro-CT owing to the limited field of view.

images from single-snapshot radiography and axial images from cone-beam CT, multidetector CT, and micro-CT. The conspicuity of the embolic agent was assessed at baseline, before starting embolization, and at the delivery end point in five sites, as follows: tumor, tumor-feeding arteries, ipsilateral liver, hepatic artery (including proper, right and/or left hepatic arteries), and contralateral (right) liver lobe (Fig 1). All five sites were included in the qualitative and quantitative image analysis for an exhaustive assessment (below). Our study design did not include pre-TAE multidetector CT and micro-CT because the contralateral healthy liver was determined to be sufficient as a baseline for comparison.

**Qualitative image analysis.**—Qualitative image analysis was performed independently by three observers (two residents in radiology and an interventional radiologist who specialized in abdominal imaging with 8 years of experience [V.T., J.C., and R.D., respectively]) in a blinded fashion. The assessment was made during the same reading session to ensure careful comparison of pre- and postembolization findings. The visibility of the embolic agent was graded as follows: 1 = definitely not visible, 2 = doubtful, and 3 = visible. Each observer recorded scores for the five anatomic sites with all imaging modalities.

**Quantitative image analysis.**—Quantitative assessment of embolic agent visibility was performed by using mean pixel intensity measurements in a square ROI. To achieve consistency, a square ROI was used for all imaging modalities, and the size was adapted to each image type resolution to analyze a 4-mm<sup>2</sup> portion of the rabbit liver (ie, a square ROI of 26 × 26 pixels for single-snapshot images, 4 × 4 pixels for cone-beam CT scans, 4 × 4 pixels for multidetector CT scans, and 235 × 235 pixels for micro-CT scans). The ROIs were placed at the same position on all pre- and postembolization images for all imaging modalities (Fig 1). The comparison was done in terms of the signal-to-noise ratio (SNR), where the mean pixel intensity (*I*) of each ROI was divided by the standard

deviation (SD) of the “estimated noise” as shown in Equation (1):

$$SNR(ROI) = \frac{\text{Mean } I(ROI)}{SD I(\text{"noise"})} \quad (1)$$

The estimated noise was calculated by using the same-size ROI positioned in

a representative location on the same image frame (for projection images) or section level (for cross-sectional images) where the signal measurement was done. Specifically, estimated noise ROIs were located in the umbilical area of the abdomen for projection images

**Table 3**  
Qualitative and Quantitative Visibility Assessment according to Imaging Modality

Imaging Modality and Group	No. of Definitely Visible Cases			SNR Measurements		
	Before Embolization*	After Embolization*†	PValue	Median SNR Change (%)	Cases with SNR Improvement*	PValue‡
<b>Single-snapshot radiography (intraoperative)</b>						
Radiopaque microsphere	0/75	27/75 (36)	<.001	-11.7	5/25	.251
Radiopaque microsphere plus contrast material	0/75	41/75 (55)	<.001	-3.5	11/25	.349
Nonradiopaque microsphere plus contrast material	0/75	53/75 (71)	<.001	-1.2	10/25	.314
<b>Cone-beam CT (intraoperative)</b>						
Radiopaque microsphere	0/75	56/75 (75)	<.001	6.5	17/25	.004
Radiopaque microsphere plus contrast material	0/75	44/75 (59)	<.001	8.6	22/25	<.001
Nonradiopaque microsphere plus contrast material	0/75	49/75 (65)	<.001	-8.9	9/25	.04
<b>Multidetector CT (1 hour after embolization)</b>						
Radiopaque microsphere	0/75	50/75 (67)	<.001	33.6	23/25	<.001
Radiopaque microsphere plus contrast material	0/75	52/75 (69)	<.001	16.0	18/25	.004
Nonradiopaque microsphere plus contrast material	0/75	27/75 (36)	<.001	16.4	21/25	<.001
<b>Micro-CT (3–5 weeks after sacrifice)§</b>						
Radiopaque microsphere	0/60	39/60 (65)	<.001	78.4	17/20	<.001
Radiopaque microsphere plus contrast material	0/60	48/60 (80)	<.001	79.7	18/20	<.001
Nonradiopaque microsphere plus contrast material	0/60	0/60 (0)	.999	38.6	17/20	<.001

Note.—Multidetector CT and micro-CT were performed only after embolization. A nonembolized contralateral liver tissue region was selected to represent the before embolization measurement.

\* Numbers are raw data.

† Numbers in parentheses are percentages.

‡ Comparison of pre- and postembolization SNR measurements.

§ Nontarget embolization evaluation was not performed owing to the limited field of view.

and in the paraspinal muscles for cone-beam CT and multidetector CT images. For micro-CT images, because of the absence of a nonliver structure for SNR measurements, the contralateral healthy liver was used to estimate noise. The SNR change, which was expressed as a percentage for all imaging modalities, was calculated on the basis of the SNR before and after embolization, as shown in Equation (2) (29):

$$\text{SNR (ROI)Change} = \frac{[\text{SNR (ROI)Post} - \text{SNR (ROI)Pre}]}{\text{SNR (ROI)Pre}} \times 100. \quad (2)$$

Furthermore, SNRs before and after embolization were compared to assess whether SNR increased. This was recorded as a binary variable for each anatomic location and for each imaging modality. Because of the limited field of view of micro-CT, nontarget embolization evaluation was not performed in the qualitative or quantitative analysis for this imaging modality.

### Statistics

Rabbit characteristics are summarized as medians and ranges. The Kruskal-Wallis test was used to compare rabbit characteristics across the groups. The Mann-Whitney *U* test was used to further explore the differences among the groups. Visibility scores of 3 (definitely visible) for each image (single-snapshot radiography, cone-beam CT, multidetector CT, and micro-CT) were counted up for each rabbit group. The counts before and after embolization were then compared with the Fisher exact test. SNRs obtained before and after embolization were compared with the Wilcoxon signed rank test. The binary variables indicating whether SNR increased after head delivery were summed and reported as counts for each rabbit group. Two-tailed  $P < .05$  was considered indicative of a statistically significant difference. The repeated measures data from qualitative and quantitative image analysis categorized according to microsphere type and anatomic location (Table 2) and microsphere type and imaging modality (Table 3) were reported.

Statistical analysis was performed with software (R: Statistical Programming Language, version 3.8.0; R Project for Statistical Computing, Vienna, Austria).

### Results

VX2 tumor growth within the left hepatic lobe was successful in all rabbits. The median maximum diameter of the

implanted tumor was 3.0 cm (range, 1.3–4.9 cm), with no significant difference in tumor size among the groups ( $P = .76$ , Table 1). All 15 rabbits underwent successful intra-arterial catheterization and embolization. A median of 0.3 mL (range, 0.05–0.3 mL) of radiopaque microspheres, 0.05 mL (range, 0.05–0.2 mL) of radiopaque microspheres, and 0.3 mL (range, 0.15–1 mL) of

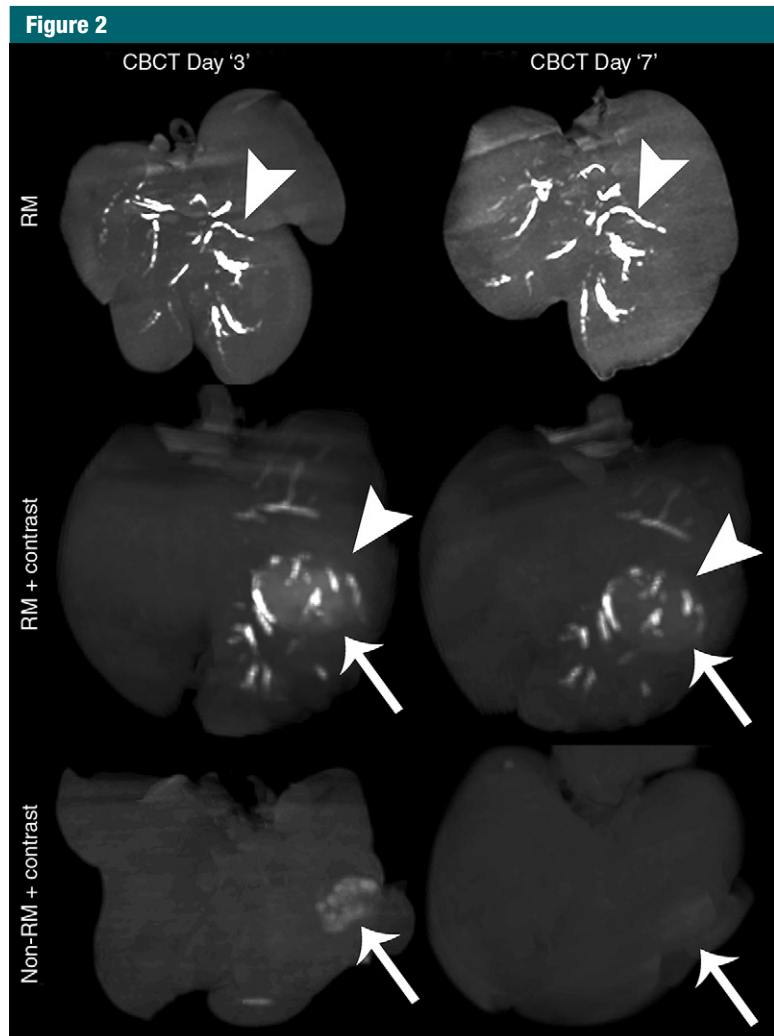


**Figure 2:** Anterior views of three-dimensional maximum intensity projection cone-beam CT (CBCT) scans of representative rabbit livers from the three treatment groups 3 and 7 days after embolization. In radiopaque microsphere (RM) group, attenuation of tumor-feeding arteries caused by radiopaque microspheres (arrowheads) at day 3 remained unchanged at day 7. In radiopaque microsphere plus contrast material group, persistence over time of radiopaque microspheres (arrowheads) was also observed, whereas a progressive washout of contrast material was noticed at day 7 compared with day 3 (arrows). In nonradiopaque microsphere plus contrast material group, only the contrast material–enhanced tumor (arrows) was visualized at day 3, with almost complete washout at day 7.



nonradiopaque microspheres was successfully injected in the radiopaque microsphere, radiopaque microsphere plus contrast material, and nonradiopaque microsphere plus contrast material groups, respectively ( $P = .03$ , Kruskal-Wallis) according to the embolization procedure end point, with significantly reduced microspheres injected in the radiopaque microsphere plus contrast

material group compared with the nonradiopaque microsphere plus contrast material group ( $P = .016$ , Mann-Whitney  $U$  test). The rabbit characteristics reported according to group are detailed in Table 1. Nontarget embolization occurred in one rabbit each in the radiopaque microsphere plus contrast material and nonradiopaque microsphere plus contrast material groups and in two rabbits

in the radiopaque microsphere group. Figures 2–6 illustrate three representative rabbits in each group and show typical results obtained with each imaging modality and at histologic analysis.

### Ex Vivo Analysis

**Cone-beam CT.**—The radiopaque microspheres remained visible and similarly located in the tumor-feeding arteries

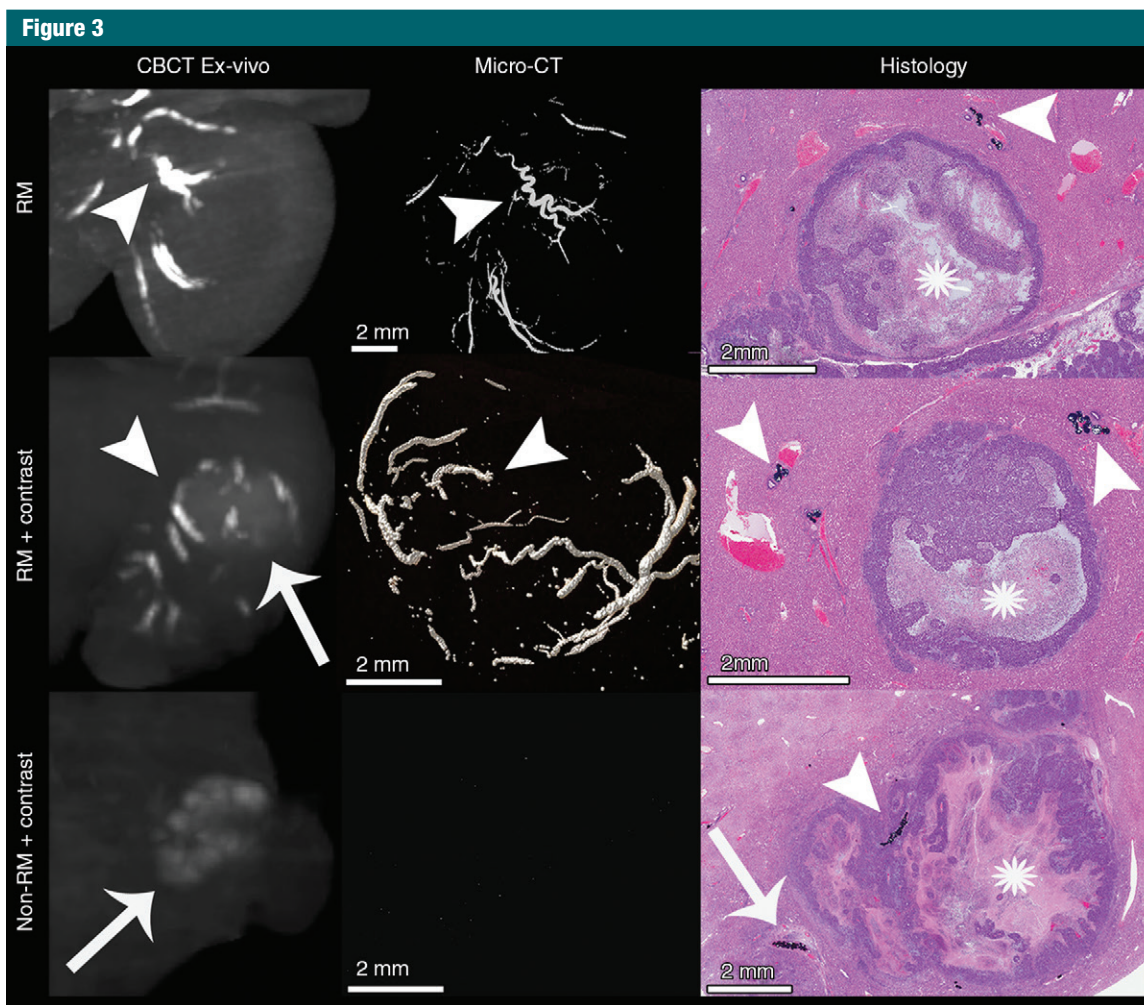


**Figure 3:** Three-dimensional reconstructed maximum intensity projection cone-beam CT (CBCT) scans, micro-CT scans (anterior view of three-dimensional maximum intensity projection), and photomicrographs (slice at maximum tumor diameter) of representative ex vivo livers from each group. For radiopaque microsphere (RM) group, proximal tumor-feeding arteries showed attenuation by radiopaque microspheres on cone-beam CT and micro-CT images (arrowheads). Radiopaque microsphere location was confirmed on photomicrograph (arrowhead). Similar results were obtained in radiopaque microsphere plus contrast material group, with additional tumor enhancement seen on cone-beam CT scan (arrow). Microspheres were detected in distal feeding arteries at tumor periphery and in surrounding liver (arrowheads). Nonradiopaque microsphere plus contrast material group showed contrast material enhancement of tumor on cone-beam CT scan (arrow). No microspheres were visualized on cone-beam CT or micro-CT scans, whereas they were detected on photomicrograph in tumor (arrowhead) and its tumor-feeding arteries (arrow). The lack of any attenuation on micro-CT image was due to contrast material washout over time. Note that center of VX2 tumor (\*) is typically necrotic, as shown on photomicrographs.

Figure 4

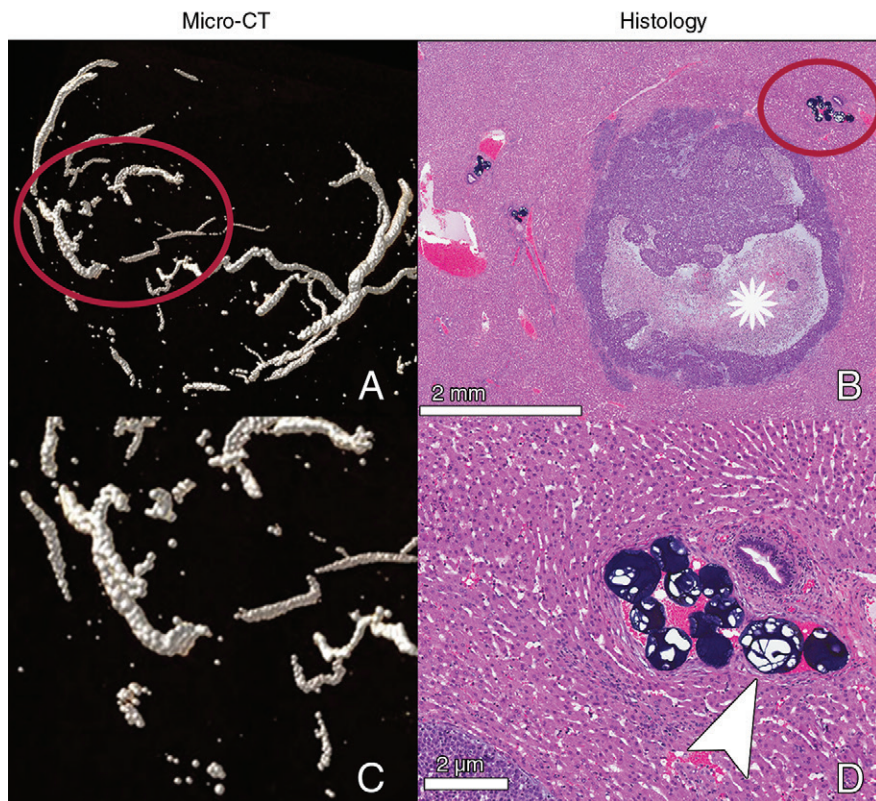


**Figure 4:** Images from same case as in Figure 3 from radiopaque microsphere plus contrast material group, with focus on visibility of radiopaque microspheres accumulated in tumor-feeding arteries. *C* and *D* are magnifications of areas circled in red on *A*, and *B*, respectively. Micro-CT scans demonstrate spatial distribution of each radiopaque microsphere within tumor-feeding arteries. Radiopaque microspheres were aligned in a single file as well as stacked by two or more beads across arterial diameter. In addition, infrequent single radiopaque microspheres were identified within more distal feeding arteries (as seen in *C*). Photomicrographs show radiopaque microspheres accumulated in tumor-feeding arteries. Magnification at level of 200  $\mu\text{m}$  shows ethiodized oil droplets in radiopaque microspheres (arrowhead). \* = Central VX2 tumor necrosis.

at days 3 and 7 in the radiopaque microsphere and radiopaque microsphere plus contrast material groups. The soluble contrast material was visualized at day 3; however, it was less visible at day 7 owing to washout in the radiopaque microsphere plus contrast material and nonradiopaque microsphere plus contrast material groups (Fig 2).

**Histologic examination.**—The location of microspheres in the embolized tumor and adjacent liver parenchyma was confirmed with histologic examination. The microspheres showed a similar distribution in the tumor rim, tumor-feeding arteries, and surrounding liver, with no statistically significant difference

among the groups. As shown in Figures 3 and 4, the microspheres were tightly packed within the hepatic and tumor-feeding arteries. In larger, more central arteries, numerous microspheres were seen filling the entire diameter of these vessels, whereas in smaller, more peripheral arteries, they were seen in a single-file arrangement filling and occluding the vessel diameter. Droplets of ethiodized oil were identified in the radiopaque microspheres (Fig 4).

#### Imaging Analysis

**Qualitative assessment.**—Radiopaque microspheres were visible at all evaluated anatomic locations after

embolization (Table 2). No embolic attenuation was seen by the three observers before embolization with pre-TAE imaging modalities for all groups (Table 3). After TAE, the embolic solutions became significantly “visible” in all groups with all imaging modalities, except on micro-CT scans in the non-radiopaque microsphere plus contrast material group (Table 3, Figs 5 and 3, respectively). Indeed, the nonradiopaque microspheres remained “not visible” on micro-CT scans (Table 3, Fig 3). The micro-CT–evidenced radiopaque microsphere distribution aligned into tumor-feeding arteries to the level of individual microsphere in a single file as well as packed by two or more across the arterial diameter (Figs 3, 4). Importantly, radiopaque microspheres were qualitatively visible with all radiologic modalities without the need for additional soluble contrast material (Figs 3, 5, 6).

**Quantitative assessment.**—The radiopaque microsphere and radiopaque microsphere plus contrast material groups demonstrated a significant increase in SNR after embolization in the tumor, feeding arteries, hepatic arteries, and nontarget tissues (Table 2). The analysis of SNR changes did not show any significant difference among groups on images from single-snapshot radiography (Table 3). However, significant SNR increases were observed on postembolization cone-beam CT, multi-detector CT, and micro-CT scans compared with pre-embolization images in all groups (Table 3).

#### Discussion

The main finding of our study is that the radiopaque microspheres were qualitatively visible at single-snapshot radiography, cone-beam CT, multi-detector CT, and micro-CT after TAE of VX2 liver tumors in the rabbit model, with or without co-administered contrast medium. This is a key development for drug-eluting bead–based intra-arterial therapies and may provide a dual benefit: (a) The visibility of radiopaque microspheres could offer immediate intraprocedural feedback regarding their localization, and (b)

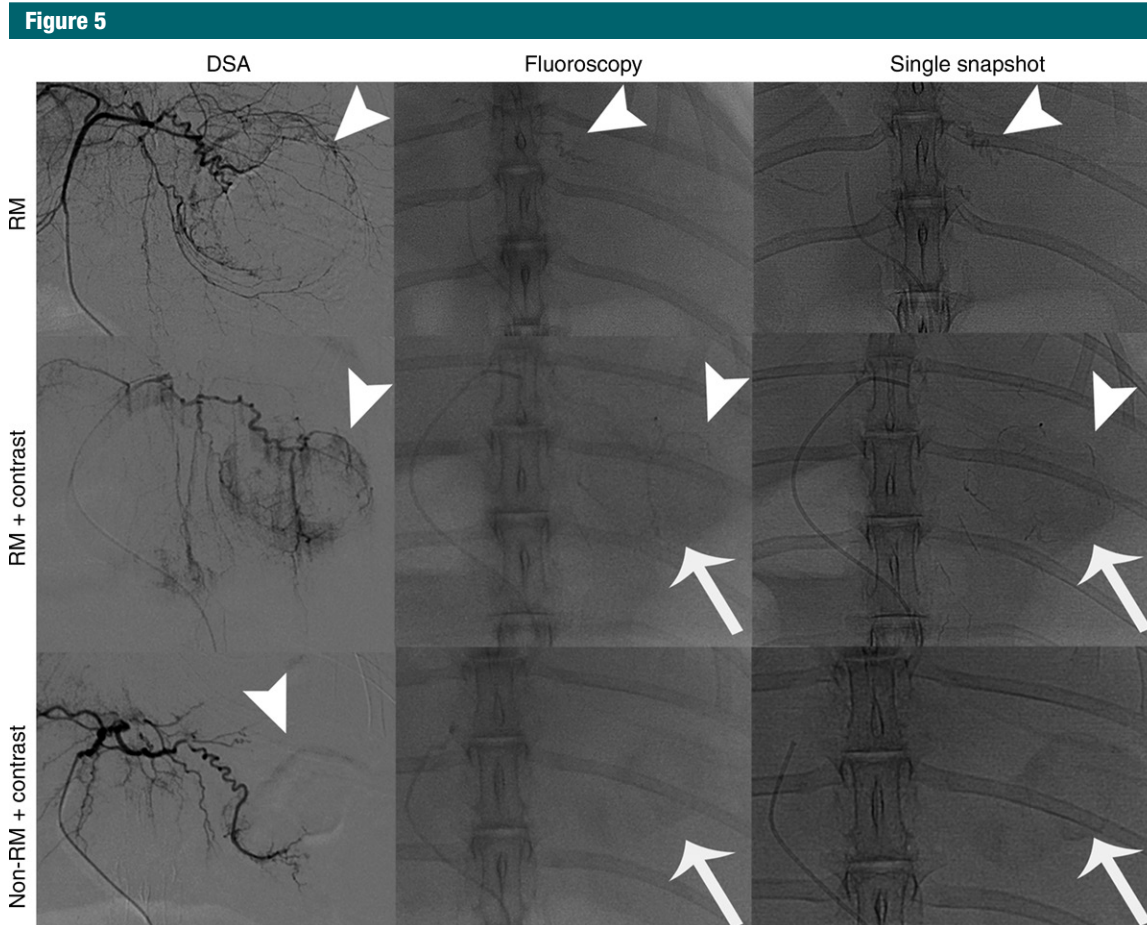


**Figure 5:** Images from digital subtraction angiography (*DSA*) (anteroposterior view), fluoroscopy (anteroposterior view), and single-snapshot radiography (anteroposterior view) in three representative rabbits from each treatment group. Digital subtraction angiography helped identify tumor location (arrowheads) and vascular anatomy. For radiopaque microsphere (*RM*) group, tumor-feeding arteries were evidenced by radiopaque microspheres—as seen on images from fluoroscopy and single-snapshot radiography (arrowheads). Similar results were obtained in radiopaque microsphere plus contrast material group, with additional tumor staining owing to soluble contrast material (arrows). Radiopaque microspheres were detected in distal tumor-feeding arteries at tumor periphery (arrowheads). Images in nonradiopaque microsphere plus contrast material group show tumor staining by soluble contrast material (arrows); however, no microspheres could be identified.

because of their long-lasting retention after embolization (ie, after soluble contrast material washout), the visibility of radiopaque microspheres could be exploited for follow-up imaging, thus helping predict therapy response in a similar way to ethiodized oil in conventional TACE (30). This is a clear advantage over existing radiolucent microspheres. In current clinical practice, interventional radiologists indirectly assume the distribution of radiolucent microspheres during embolization by the visualization of retained soluble contrast material and/or the lack of tumor contrast enhancement.

Intraprocedural cone-beam CT techniques such as dual-phase or unenhanced cone-beam CT may help highlight tumor devascularization or tumor margin contrast material saturation, respectively, during or after TACE with drug-eluting beads and enable intraprocedural assessment of treatment delivery (22,23,31). However, because of contrast material washout, these signs are temporary and limit postprocedural evaluation over time.

Qualitative visibility of radiopaque microspheres alone was limited under real-time fluoroscopy during delivery. Only groupings of radiopaque

microspheres (and not individual microspheres) were visible to the interventional radiologists, potentially limiting the threshold of detection of nontarget embolization. Multidetector CT, cone-beam CT, and micro-CT demonstrated significant qualitative and quantitative visibility differences after TAE, whereas single-snapshot images failed to show any quantitative postprocedural changes. A possible explanation could be related to the projection nature of the single-snapshot images, which carries less information compared with three-dimensional datasets of cross-sectional

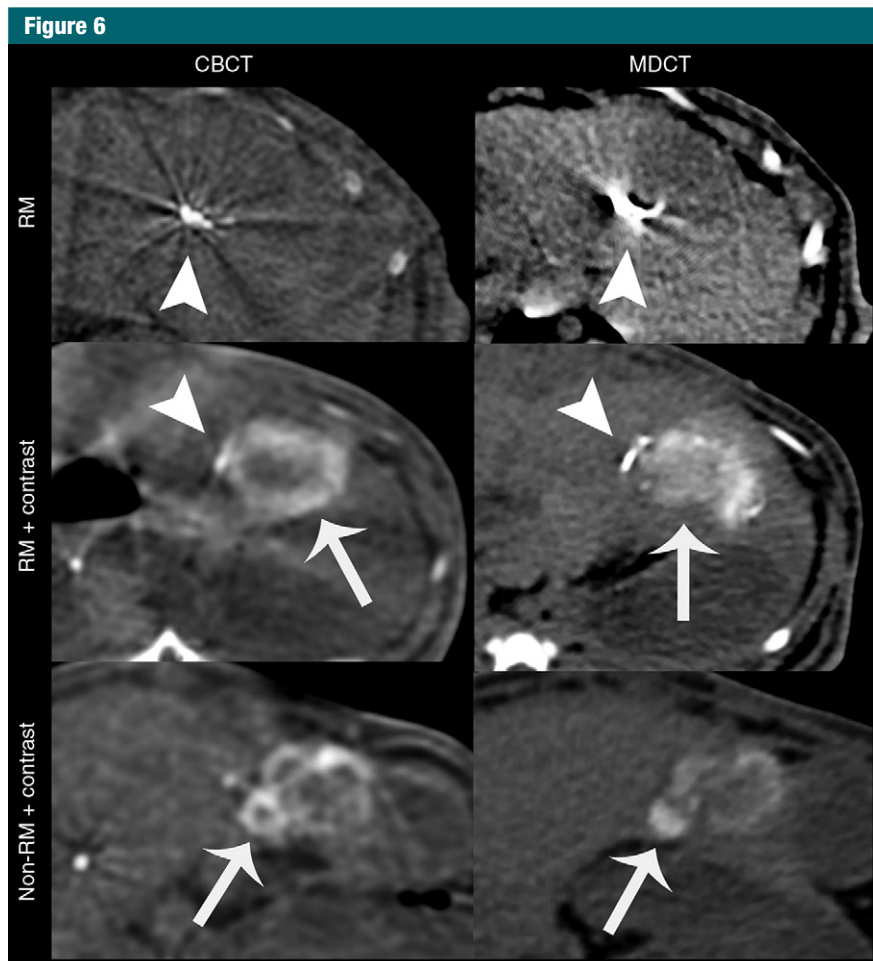


**Figure 6:** Axial cone-beam CT (CBCT) and multidetector CT (MDCT) scans in representative rabbits from each treatment group. For radiopaque microsphere (RM) group, proximal tumor-feeding arteries filled with radiopaque microspheres showed strong attenuation (arrowheads) on cone-beam CT and multidetector CT scans. Tumor for the radiopaque microsphere plus contrast material group was seen as hypoattenuating nodular structure compared with nontumoral hepatic parenchyma (arrows). Similar results were obtained in radiopaque microsphere plus contrast material group, with additional tumor enhancement owing to soluble contrast material (arrows). Microspheres were detected more distally in feeding arteries at tumor periphery (arrowheads). Images in nonradiopaque microsphere plus contrast material group show tumor enhancement by contrast material (arrows); however, no microspheres were detected. Note that VX2 tumors showed typical low attenuation centrally owing to necrosis.

imaging (32). The number of cases of SNR increase after embolization was higher for multidetector CT and micro-CT compared with cone-beam CT. For cone-beam CT, the motorized C-arm covers a total angular range of 240° for each scan and so produces a limited angle reconstruction. This elevates the noise compared with multidetector CT and/or micro-CT, where the scans are 360°. Furthermore, the

acquisition time for cone-beam CT was 10 seconds, which allowed for three to five breaths to enter the acquisition time window. Multidetector CT captured the entire scan in 0.5 second with minimal motion-related artifacts, whereas the liver at micro-CT is static. Taken together, decreased image quality for cone-beam CT could have led to less precise ROI placement and SNR measurement.

Although micro-CT cannot be implemented in the clinic, this modality was chosen to demonstrate the precise imaging location of radiopaque microspheres. The provided resolution was able to evidence the exact radiopaque microsphere distribution, even at a single microsphere level. In addition, and more importantly, contrast material washout over time could be seen in the radiopaque microsphere plus contrast material group, which clearly demonstrates that the attenuation evidenced on the images could be attributed to the radiopaque microspheres.

Because radiopaque microspheres are denser than saline, they tended to settle in the injection syringe (ethiodized oil density: 1.3 g/cm<sup>3</sup> vs water density: 1 g/cm<sup>3</sup>). Although care was taken to mitigate microsphere sedimentation in saline with constant movement and rotation of the syringe during delivery, clumping of the radiopaque microspheres often resulted. Thus, a more proximal embolization could have occurred in the radiopaque microsphere group and may be the reason for the higher incidence of nontarget embolization. Better suspension of the radiopaque microspheres was obtained in the radiopaque microsphere plus contrast material group because of the higher density and viscosity of soluble contrast medium compared with saline. This may have reduced radiopaque microsphere aggregation. Despite a more proximal embolization observed with radiopaque microspheres, the quantitative analysis also demonstrated that SNR measurements increased significantly in the tumor and its feeding arteries, which reflects the ethiodized oil–related attenuation of the radiopaque microspheres and highlights the fact that these microspheres were able to reach distal regions in the embolized tissues, as confirmed at pathologic examination. It is surprising that no significant quantitative changes were observed in the tumor in the nonradiopaque microsphere plus contrast material group, which could be related to the “washout” of the soluble contrast material.

Our study has several limitations. First, we did not perform an extended

in vivo follow-up to evaluate long-term visibility of radiopaque microspheres. Second, the embolic effects of radiopaque microspheres were not estimated and compared with those of radiolucent microspheres. Third, the reaction of the surrounding tissue to the radiopaque microspheres was not evaluated and further experimental studies are needed. Fourth, experiments were performed with microspheres unloaded with a chemotherapeutic agent. Although ethiodized oil–loaded microspheres can also be loaded with chemotherapy (26), our study was designed to investigate the potential added value of radiopaque microspheres loaded with ethiodized oil over beads in terms of visibility. Fifth, a quantitative estimation of the distribution of radiopaque microspheres into the tumors was not performed. Indeed, the addition of spectral imaging may help quantify the amount of iodine in a volume of interest and therefore provide the amount of radiopaque microspheres in that volume (33). However, this was beyond the scope of the study, which was focused on the visibility of radiopaque microspheres.

In conclusion, radiopaque microspheres were visible with multiple radiologic imaging modalities during TAE in the VX2 rabbit liver tumor model and increased conspicuity of tumor location and tumor-feeding arteries. Further work is required to characterize any potential clinical benefits of such additional information and to use the contrast material density measured in radiopaque microspheres as a marker of drug delivery by correlating Hounsfield units with drug concentration in tumors.

**Disclosures of Conflicts of Interest:** V.T. disclosed no relevant relationships. R.D. disclosed no relevant relationships. M.L. Activities related to the present article: is an employee of Philips. Activities not related to the present article: disclosed no relevant relationships. Other relationships: disclosed no relevant relationships. J.H.S. Activities related to the present article: none to disclose. Activities not related to the present article: none to disclose. Other relationships: none to disclose. K.V.S. Activities related to the present article: receives research funding through a cooperative research and development agreement between NIH and Biocompatibles.

Activities not related to the present article: is a consultant and speaker for Biocompatibles. Other relationships: disclosed no relevant relationships. Z.W. disclosed no relevant relationships. J.C. disclosed no relevant relationships. C.G.J. Activities related to the present article: receives research funding through a cooperative research and development agreement between NIH and Biocompatibles. Activities not related to the present article: disclosed no relevant relationships. Other relationships: disclosed no relevant relationships. N.B. disclosed no relevant relationships. M.R.D. Activities related to the present article: is an employee of Biocompatibles. Activities not related to the present article: disclosed no relevant relationships. Other relationships: disclosed no relevant relationships. D.S. Activities related to the present article: disclosed no relevant relationships. Activities not related to the present article: is employed by Philips Research; has a patent with Philips Research. Other relationships: disclosed no relevant relationships. D.L.W. disclosed no relevant relationships. A.L.L. Activities related to the present article: is employed by Biocompatibles. Activities not related to the present article: disclosed no relevant relationships. Other relationships: has a patent pending. Y.T. Activities related to the present article: disclosed no relevant relationships. Activities not related to the present article: is an employee of Biocompatibles. Other relationships: disclosed no relevant relationships. M.G. Activities related to the present article: disclosed no relevant relationships. Activities not related to the present article: is employed by Philips Research, has patents with Philips Research. Other relationships: disclosed no relevant relationships. B.J.W. Activities related to the present article: disclosed no relevant relationships. Activities not related to the present article: disclosed no relevant relationships. Other relationships: has a patent pending. J.F.G. Activities related to the present article: institution received a grant from Philips. Activities not related to the present article: institution received money from Nordion, Bayer Healthcare, DOB, Biocompatibles/BTG, Context Vision, and Gurbet. Other relationships: disclosed no relevant relationships.

## References

- Parkin DM, Bray F, Ferlay J, Pisani P. Estimating the world cancer burden: Globocan 2000. *Int J Cancer* 2001;94(2):153–156.
- Bruix J, Sherman M, Llovet JM, et al. Clinical management of hepatocellular carcinoma. Conclusions of the Barcelona-2000 EASL conference. European Association for the Study of the Liver. *J Hepatol* 2001;35(3):421–430.
- Schwartz M. Liver transplantation for hepatocellular carcinoma. *Gastroenterology* 2004;127(5 Suppl 1):S268–S276.
- Yao FY, Bass NM, Nikolai B, et al. Liver transplantation for hepatocellular carcinoma: analysis of survival according to the intention-to-treat principle and dropout from the waiting list. *Liver Transpl* 2002;8(10):873–883.
- Cammà C, Schepis F, Orlando A, et al. Transarterial chemoembolization for unresectable hepatocellular carcinoma: meta-analysis of randomized controlled trials. *Radiology* 2002;224(1):47–54.
- Llovet JM, Bruix J. Systematic review of randomized trials for unresectable hepatocellular carcinoma: chemoembolization improves survival. *Hepatology* 2003;37(2):429–442.
- Takayasu K, Arii S, Ikai I, et al. Prospective cohort study of transarterial chemoembolization for unresectable hepatocellular carcinoma in 8510 patients. *Gastroenterology* 2006;131(2):461–469.
- Llovet JM, Fuster J, Bruix J; Barcelona-Clinic Liver Cancer Group. The Barcelona approach: diagnosis, staging, and treatment of hepatocellular carcinoma. *Liver Transpl* 2004;10(2 Suppl 1):S115–S120.
- Sahara S, Kawai N, Sato M, et al. Prospective evaluation of transcatheter arterial chemoembolization (TACE) with multiple anti-cancer drugs (epirubicin, cisplatin, mitomycin c, 5-fluorouracil) compared with TACE with epirubicin for treatment of hepatocellular carcinoma. *Cardiovasc Intervent Radiol* 2012;35(6):1363–1371.
- Tam KY, Leung KC, Wang YX. Chemoembolization agents for cancer treatment. *Eur J Pharm Sci* 2011;44(1-2):1–10.
- Mabed M, Esmaeel M, El-Khodary T, Awad M, Amer T. A randomized controlled trial of transcatheter arterial chemoembolization with lipiodol, doxorubicin and cisplatin versus intravenous doxorubicin for patients with unresectable hepatocellular carcinoma. *Eur J Cancer Care (Engl)* 2009;18(5):492–499.
- Gaba RC, Baumgarten S, Omene BO, et al. Ethiodized oil uptake does not predict doxorubicin drug delivery after chemoembolization in VX2 liver tumors. *J Vasc Interv Radiol* 2012;23(2):265–273.
- Sharma KV, Dreher MR, Tang Y, et al. Development of “imageable” beads for transcatheter embolotherapy. *J Vasc Interv Radiol* 2010;21(6):865–876.
- Biondi M, Fusco S, Lewis AL, Netti PA. New insights into the mechanisms of the interactions between doxorubicin and the ion-exchange hydrogel DC Bead for use in transarterial chemoembolization (TACE). *J Biomater Sci Polym Ed* 2012;23(1-4):333–354.
- Horák D, Svec F, Kálal J, et al. Hydrogels in endovascular embolization. II. Clinical use of spherical particles. *Biomaterials* 1986;7(6):467–470.

16. Horák D, Svec F, Kálal J, et al. Hydrogels in endovascular embolization. IV. Effect of radiopaque spherical particles on the living tissue. *Biomaterials* 1988;9(4):367–371.
17. Horák D, Cervinka M, Půza V. Hydrogels in endovascular embolization. VI. Toxicity tests of poly(2-hydroxyethyl methacrylate) particles on cell cultures. *Biomaterials* 1997;18(20):1355–1359.
18. Song MJ, Chun HJ, Song S, et al. Comparative study between doxorubicin-eluting beads and conventional transarterial chemoembolization for treatment of hepatocellular carcinoma. *J Hepatol* 2012;57(6):1244–1250.
19. Lewis AL, Taylor RR, Hall B, Gonzalez MV, Willis SL, Stratford PW. Pharmacokinetic and safety study of doxorubicin-eluting beads in a porcine model of hepatic arterial embolization. *J Vasc Interv Radiol* 2006;17(8):1335–1343.
20. Namur J, Citron SJ, Sellers MT, et al. Embolization of hepatocellular carcinoma with drug-eluting beads: doxorubicin tissue concentration and distribution in patient liver explants. *J Hepatol* 2011;55(6):1332–1338.
21. Varela M, Real MI, Burrell M, et al. Chemoembolization of hepatocellular carcinoma with drug eluting beads: efficacy and doxorubicin pharmacokinetics. *J Hepatol* 2007;46(3):474–481.
22. Suk Oh J, Jong Chun H, Gil Choi B, Gyu Lee H. Transarterial chemoembolization with drug-eluting beads in hepatocellular carcinoma: usefulness of contrast saturation features on cone-beam computed tomography imaging for predicting short-term tumor response. *J Vasc Interv Radiol* 2013;24(4):483–489.
23. Loffroy R, Lin M, Yenokyan G, et al. Intra-procedural C-arm dual-phase cone-beam CT: can it be used to predict short-term response to TACE with drug-eluting beads in patients with hepatocellular carcinoma? *Radiology* 2013;266(2):636–648.
24. Vogl TJ, Lammer J, Lencioni R, et al. Liver, gastrointestinal, and cardiac toxicity in intermediate hepatocellular carcinoma treated with PRECISION TACE with drug-eluting beads: results from the PRECISION V randomized trial. *AJR Am J Roentgenol* 2011;197(4):W562–W570.
25. Lammer J, Malagari K, Vogl T, et al. Prospective randomized study of doxorubicin-eluting-bead embolization in the treatment of hepatocellular carcinoma: results of the PRECISION V study. *Cardiovasc Intervent Radiol* 2010;33(1):41–52.
26. Dreher MR, Sharma KV, Woods DL, et al. Radiopaque drug-eluting beads for transcatheter embolotherapy: experimental study of drug penetration and coverage in swine. *J Vasc Interv Radiol* 2012;23(2):257–64.e4.
27. Dreher MR, Wood BJ, Negussie AH, Lewis A, Tang WO. Imaging embolic microspheres. U.S. patent 14/152488 A2. Filed March 14, 2014.
28. Lee KH, Liapi E, Buijs M, et al. Percutaneous US-guided implantation of Vx-2 carcinoma into rabbit liver: a comparison with open surgical method. *J Surg Res* 2009;155(1):94–99.
29. Stampfl U, Sommer CM, Bellemann N, et al. Multimodal visibility of a modified polyzene-F-coated spherical embolic agent for liver embolization: feasibility study in a porcine model. *J Vasc Interv Radiol* 2012;23(9):1225–31.e2.
30. Takayasu K, Muramatsu Y, Maeda T, et al. Targeted transarterial oily chemoembolization for small foci of hepatocellular carcinoma using a unified helical CT and angiography system: analysis of factors affecting local recurrence and survival rates. *AJR Am J Roentgenol* 2001;176(3):681–688.
31. Tacher V, Radaelli A, Lin M, Geschwind JF. How I do it: cone-beam CT during transarterial chemoembolization for liver cancer. *Radiology* 2015;274(2):320–334.
32. Paul J, Jacobi V, Farhang M, Bazrafshan B, Vogl TJ, Mbalisike EC. Radiation dose and image quality of x-ray volume imaging systems: cone-beam computed tomography, digital subtraction angiography and digital fluoroscopy. *Eur Radiol* 2013;23(6):1582–1593.
33. Tacher V, Schirra CO, Thran A, et al. Quantitative image feedback in TACE: combining novel imageable beads and spectral CT. Presented at the 38th Annual Meeting of the Society of Interventional Radiology, New Orleans, La, April 13–18, 2013.